express
polymer letters

Research article

Nanostructures and toughening mechanisms in lightly cross-linked all-methacrylate copolymer/functional block copolymer blends

Hajime Kishi* , *Ayana Kubo, Yohei Miyaji, Ayu Mochizuki, Ryoko Hara, Katsuya Tanaka, Takeshi Kakibe* , *Satoshi Matsuda*

Graduate School of Engineering, University of Hyogo, 2167, Shosha, Himeji, Hyogo, 671-2201, Japan

Abstract. Functional triblock copolymers (BCPs), *i.e.*, poly(glycidyl methacrylate/methyl methacrylate)-*b*-poly(lauryl methacrylate)-*b*-poly(glycidyl methacrylate/methyl methacrylate) triblock copolymers [(P(GMA/MMA)-*b*-PLMA-*b*-P(GMA/MMA)], were investigated as toughening modifiers for all-methacrylate polymer blends. Methyl methacrylate (MMA) was copolymerized with methacrylic acid (MAA) in the presence of the BCPs. Without MAA in the polymethacrylate matrices, the BCP blends formed micron-scale phase structures by polymerization-induced phase separation. In matrices copolymerized with MAA, self-assembled nanostructures, such as curved lamellae, worm-like cylindrical micelles, or spherical micelles were formed. The BCP blends with worm-like cylindrical nano-micelles achieved much higher fracture toughness than those with spherical nano-micelles. The toughening mechanisms were elucidated by transmission electron microscopy. Cavitation was initiated in worm-like cylindrical nano-micelles, and the aligned cavitation formed craze-like deformation with increased loads. This relieves hydrostatic tensile stress in front of the crack tip, forming a large shear yield zone within the craze-like deformation region, contributing to high toughness.

Keywords: triblock copolymer, cavitation, polymer blends, nanostructures, toughening

1. Introduction

Poly(methyl methacrylate) (PMMA) has high transparency and a high modulus of elasticity and is therefore used in a variety of applications, such as interior materials. Methacrylate copolymers can also be produced with a range of functional monomers, allowing the mechanical and thermal properties of the polymeric materials to be easily controlled [1–3]. PMMA, however, is a relatively brittle polymer and numerous attempts have been made to increase its toughness by incorporating rubbery components [4–8], with the aim of using it in more structural applications. In addition, second-generation acrylic adhesives (SGAs) are important applications for methacrylate polymers due to their advantageous

properties, such as balanced shear/peel adhesive strength and efficient curing productivity at room temperature via redox reaction [9–11]. Current SGAs are composed of acrylic monomers and elastomers, and form micron-scale phase structures through polymerization-induced phase separation [11].
The addition of core-shell rubber (CSR) particles is the typical toughening technique for PMMA. The shell components of the CSRs have been designed to achieve good dispersion in the PMMA during the mixing process. Cho and coworkers [7, 8] reported that the toughening mechanism of the CSR-blended PMMA in Charpy impact tests was shear yielding induced by cavitation of the rubber particles, whereas in single-edge notched bending (SENB) tests,

multiple crazing was the predominant factor. Crazes in brittle polymers, including rubber particles, consist of voids and fibrils (*i.e.*, stretched polymer chains) and occur mainly in regions of stress concentration around the equators of the rubbery spherical particles [12–16]. The toughening mechanisms have also been found to be controlled by the strain rate. When CSR particles are used as the toughening modifiers, the shape of the rubbery phases is typically spherical. Amphiphilic block copolymers (BCPs) have attracted attention as toughening modifiers for epoxy polymer blends [17–29]. Many BCPs have been synthesized to modify epoxy cured blends, and the nanostructures and mechanical properties of the blends have been studied extensively by the Bates group [17–19]. Dean *et al*. [19] reported methylene dianiline cured DGEBA/poly(ethylene oxide)-*b*-poly(butadiene) (PEO-*b*-PB). A phase change was observed from spherical micelles to branched cylindrical micelles and finally to vesicles, as the volume fraction of the epoxy-miscible PEO block decreased. Ritzenthaler and coworkers [20, 21] studied epoxy/ polystyrene-*b*-polybutadiene-*b*-poly(methyl methacrylate) triblock polymer (PS-*b*-PB-*b*-PMMA) blends. Raspberry-like nanostructures were observed in the epoxy blends cured with 4,4′-methylene-bis-(3-chloro 2,6-diethylaniline) (MCDEA). Kishi and coworkers [22, 23, 25–27] investigated phenol-novolac cured epoxy/ poly(methyl methacrylate)-*b*-poly(n-butyl acrylate)-*b*-poly(methyl methacrylate) (PMMA-*b*-PnBA-*b*-PMMA) triblock copolymer blends. The miscibility of the PMMA end blocks of the BCPs into the cured epoxy matrix was a key factor for the formation of nano-micelles [22]. Different nanostructures, such as spherical micelles, cylindrical micelles, and curved lamellae were formed in the cured epoxy blends. The shapes of the immiscible rubbery nano-micelles were controlled by varying the molecular weight of the immiscible PnBA block chain, the ratio of PnBA in the total blends, and the miscibility of the PMMA block chains in the epoxy polymers [23, 26, 27]. Small angle X-ray scattering analyses indicated that the seeds of the differently shaped nano-micelles were formed by a self-assembly mechanism [23, 24]. They also clarified that the shape of the nano-micelles had an important effect on the fracture toughness and the modulus of elasticity of the epoxy/BCP blends [25–27]. Liu and coworkers [28, 30] and Thomson *et al*. [29] discussed the differences in the toughening mechanisms with respect to the shape of

the nano-micelles in the epoxy/ poly(ethylene oxide)-*b*-poly(ethylene-alt-propylene) (PEO-*b*-PEP) BCP blends. The worm-like cylindrical micelles resulted in an improvement in toughness of over 100% compared to the pure epoxy. The toughening mechanisms were concluded to be a combination of crack tip blunting, cavitation, particle debonding, limited shear yielding, and crack bridging [30]. However, it should be noted that these epoxy polymer matrices were highly cross-linked.

In this study, we investigated BCPs consisting of chemically distinct methacrylate block chains as the toughening modifiers for room temperature polymerized lightly cross-linked methacrylate polymer blends. The phase structures of redox-polymerized methacrylate monomer/amphiphilic methacrylate BCP, *i.e.*, poly(glycidyl methacrylate/methyl methacrylate)-*b*-PLMA-*b*-poly (glycidyl methacrylate/methyl methacrylate) triblock copolymer [(P(GMA/MMA)-*b*-PLMA-*b*-P(GMA/ MMA)] blends were investigated using microscopy techniques, with respect to the degree of functionality of both the hard blocks of the BCPs and the polymethacrylate matrices. The objectives of the present study were to investigate the relationships between the phase structures and the fracture toughness of the polymerized methacrylate/BCP blends and to clarify the toughening mechanisms.

2. Experimental
2.1. Materials
MMA monomer (Tokyo Chemical Industry Co., Ltd.) was used as the main component. A small amount of methacrylic acid (MAA) monomer (Tokyo Chemical Industry Co., Ltd.) was copolymerized with the MMA to prepare the polymethacrylate matrices. These monomers were polymerized by redox reaction at room temperature. For the redox reaction initiator, trimethyl thiourea was used as the reducing agent and cumene hydroxy peroxide was used as an oxidizing agent.

P(GMA/MMA)-*b*-PLMA-*b*-P(GMA/MMA) triblock copolymers (methacrylate BCPs) were used as toughening modifiers for the polymethacrylate blends. Three types of methacrylate BCPs, differing in the GMA copolymerization ratio in the hard blocks, were synthesized by Otsuka Chemical Co., Ltd., using living radical polymerization and were used as received. The chemical structure of the methacrylate BCPs is shown in Figure 1. The molecular weight of
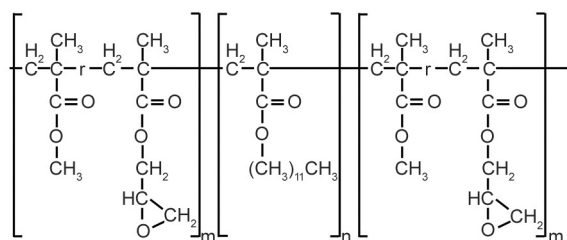
Figure 1. Chemical structure of [poly(glycidyl methacrylate/methyl methacrylate)-*b*-poly(lauryl methacrylate)-*b*-poly(glycidyl methacrylate/methyl methacrylate)], [P(GMA/MMA)-*b*-PLMA-*b*-P(GMA/MMA)], triblock copolymer (BCP).

Table 1. Weight-average molecular mass (M_w), GMA/MMA copolymerization ratio in the hard block chains, and polydispersity (M_w/M_n) of P(GMA/MMA)-*b*-PLMA-*b*-P(GMA/MMA) triblock copolymers (BCP).

BPC	Hard blocks P(GMA/MMA)	Soft block PLMA	Polydispersity (M_w/M_n)
G64M36*b*L	(12 500/5 000)×2	30 000	1.45
G43M57*b*L	(9 500/8 500)×2	30 000	1.63
G22M78*b*L	(5 000/12 500)×2	30 000	1.40

the methacrylate BCPs and the composition (GMA/MMA copolymerization ratio in the hard block chains of the methacrylate BCPs) were systematically controlled, as shown in Table 1. For example, 'G64M36*b*L' means that the copolymerized GMA/MMA molar ratio in the hard block was 64:36. The PLMA middle block chain is immiscible with the MMA/MAA copolymerized matrix polymer, while the P(GMA/MMA) hard block chains are miscible.

2.2. Size exclusion chromatography
The molecular weight distributions of the BCPs were determined using size exclusion chromatography (SEC; PU-2080 HPLC system, Jasco, with Jasco-Borwin-GPC software, which was equipped with two connected columns, Shodex LF-804 and KF-806L). Tetrahydrofuran (THF) was used as the solvent. The average molecular weights were calibrated using mono-dispersed polystyrene standards.

2.3. Redox polymerization of methacrylate monomer/amphiphilic methacrylate BCP blends
MMA/MAA monomer blends were copolymerized by redox reaction in the presence of the BCPs according to the following procedure. First, the MMA was mixed with the MAA and the BCP was dissolved into the MMA/MAA monomer blends due

stirring at room temperature for 2 h. The MAA molar ratio in the MMA/MAA blend was compared in the range of 0–3 mol%. The amount of BCP added to the blend was 5 or 10 wt%. Trimethyl thiourea as the reducing agent was added to the solution which was then mixed for 30 min. Cumene hydroxy peroxide as the oxidizing agent was then added to the solution which was mixed for another minute.

The mixture was poured into a mold pre-treated with a release agent and polymerized by redox reaction at room temperature for 20 h and then at 60 °C for 4 h. After this procedure, the oven was switched off and the polymerized methacrylate blends were allowed to cool slowly to room temperature.

2.4. Gel content of polymerized methacrylate blends
The gel content represents the degree of cross-linking in the polymerized methacrylate blends. The polymerized blend sample was covered with poly(ethylene terephthalate) cloth (mesh #380) and was soaked in THF at 22 °C for 10 days. The soluble portion of the sample was washed out and removed by filtration. The remaining solid was then dried to a constant weight. The gel fraction in the polymerized methacrylate blends was calculated using (Equation (1)):

$$\text{Gel fraction [\%]} = \frac{W_1}{W_0} \cdot 100 \tag{1}$$

where W_0 and W_1 are the sample weights before and after filtration, respectively.

2.5. Dynamic mechanical analysis of polymerized methacrylate blends
The effects of temperature on the viscoelastic properties (storage modulus E', loss modulus E'' and loss tangent $\tan\delta$) of the P(MMA/MAA) and the BCP blends were evaluated by dynamic mechanical analysis (DMA) operating in the tensile mode (DMS6000, Seiko Instruments, Inc., Japan). The dynamic frequency was 1 Hz, and each specimen had a length of 40 mm (span: 20 mm), a width of 4 mm and a thickness of 1 mm. The samples were tested over the temperature range from 25 to 200 °C at a heating rate of 2 °C/min. From these data, the rubbery plateau values of the storage modulus (E'_r) were determined, and M_c (average molecular weight between crosslinks) was calculated based on rubber elasticity theory [31] using the equation (Equation (2)) [32]:

$$M_c\,[\text{g/mol}] = \frac{3\varphi\rho RT}{E'_r} \tag{2}$$

where φ is a front factor (equivalent to the ratio of the mean square end-to-end distance of a network chain to that of a randomly coiled chain and assumed to be 1.0 [33–35]), ρ is the density of the polymer, R is the gas constant (8.31 J/(mol·K)), T is the temperature to reach the rubbery plateau region, and E'_r is the storage modulus in the rubbery plateau at the T.

2.6. Fracture toughness of polymerized methacrylate blends

The fracture toughness (critical stress intensity factor: K_{IC}) of the polymerized methacrylate blends was measured using the single-edge notched three-point bending (SEN-3PB) method according to ASTM D 5045. The specimen dimensions were 55 mm long × 12 mm wide × 6 mm thick. The span length for the flexure test was 48 mm. The initial crack length was within the range of 6.1±0.5 mm to meet the geometric requirement. The three-point bending tests were performed at a test rate of 10 mm/min at 23 °C using a universal testing machine (Autograph AGS-J 10 kN, Shimadzu, Japan). The details of the test can be found in the previous publication [22].

2.7. Microscopy observations
2.7.1. Optical microscopy
The process zones around critically and sub-critically loaded cracks in the double-notched four-point bending (DN-4PB) specimens were examined using optical microscopy (OM). The DN-4PB technique is described in detail by Sue and coworkers [36, 37, 43]. In this procedure, two nearly identical cracks are made on the same edge of a rectangular specimen. When the specimen is loaded in the four-point bending configuration until one of the cracks fails, the zone in front of the surviving crack has characteristics of the deformation behavior just before the failure. Thus, the critical crack is the one that causes failure, and the sub-critical crack is the one that does not. Since the sub-critical crack is arrested, the deformation events in the process zone around the crack tip are not erased by the final fracture process. Therefore, the DN-4PB technique is useful for examining the sequence of multiple deformation events. Polished petrographic thin sections (100 µm thick) that include the process zone in front of the sub-critical

crack tip were prepared from the mid-plane of the tested specimens. The process zones and the shear deformation bands in the thin sections were observed using an optical microscope (Eclipse E600W, Nikon, Japan) in transmission mode under both bright-field and cross-polarized conditions.

2.7.2. Scanning electron microscopy
The fracture surfaces and polished surfaces of the polymerized methacrylate blends were observed using scanning electron microscopy (SEM; VE-9800, Keyence, Japan). The samples were mounted on brass stubs and coated with a thin layer of gold using an ion sputter coater (JFC-1100E, Jeol, Japan).

2.7.3. Transmission electron microscopy
Thin sections of the polymerized methacrylate blends were cryo-microtomed at –80 °C to a thickness of 40–50 nm. Microtomed thin sections of the cured polymers were stained with RuO_4 vapor and observed using transmission electron microscopy (TEM; H-7650, Hitachi, Japan) operated at an acceleration voltage of 100 kV.

3. Results and discussion
3.1. Degree of cross-linking of polymerized MMA-MAA/functional BCP blends
Figure 2 shows the evidence of cross-linking formation in the methacrylate polymer/5 wt% BCP blends. The vertical axis shows the gel fraction in the different blends. The horizontal axis shows the GMA copolymerization ratio in the hard block chains of the blended BCPs. The MAA copolymerization ratio in the methacrylate matrix polymers was also varied. In the case of the methacrylate MMA-MAA copolymer without blended BCP, almost no gel fraction
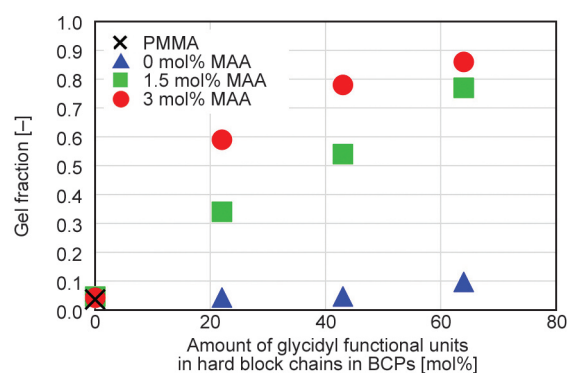

Figure 2. Gel fraction of polymerized MMA-MAA/5 wt% BCP blends.

was obtained. This means that the MMA-MAA copolymer was a linear polymer without cross-linking. The weight average molecular mass of the MMA-MAA copolymer without cross-linking was about 500 000. On the other hand, as the amounts of functional groups in both the matrix polymers and the hard block chains of the BCPs increased, the gel fraction increased. This means that MAA units reacted with the glycidyl groups of the hard blocks of the BCPs, and the polymerized MMA-MAA/functional BCP blends were lightly cross-linked.

Figure 3 shows the temperature dependence of the storage modulus (E') for the P(MMA97/MAA3) copolymer and the BCP blends. At temperatures higher than the glass transition temperatures, the P(MMA97/MAA3) copolymer showed a significant decrease (flow) in the storage modulus, while the 5 wt% BCP (G22M78bL) blend showed a rubbery plateau region. This result suggests that cross-linking has occurred due to the reaction between the glycidyl groups of the hard block chains in the BCPs and the MAA units (carboxy groups) in the matrix copolymer. The M_c for the BCP blends was 4390 g/mol, calculated using Equation (2) at the $T = 403$ K in the rubbery plateau region.
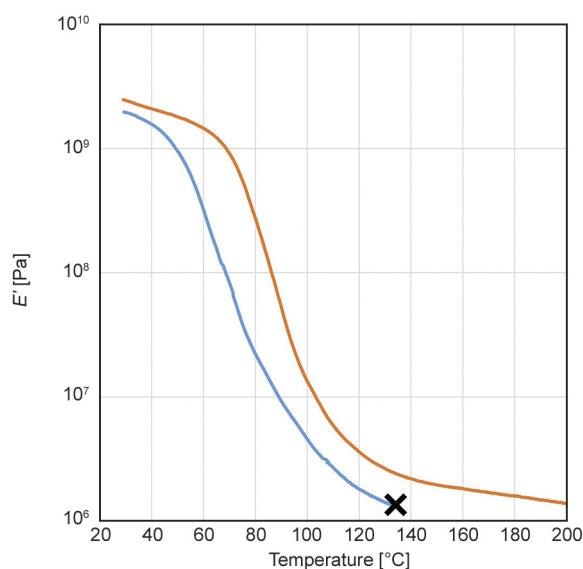

Figure 3. Temperature dependence of storage moduli E' for P(MMA97/MAA3) copolymer (blue line) and 5 wt% BCP (G22M78bL) blends (red line). The cross mark at around 130 °C for the P(MMA97/MAA3) copolymer (blue line) indicates that the sample flowed at this temperature, making it impossible to obtain viscoelastic data.

3.2. Nanostructures of polymerized MMA-MAA/functional BCP blends

The types of phase structures in the different blends can be controlled by varying the amounts of functional groups in both the methacrylate matrix polymer and the BCPs. Specifically, the GMA copolymerization ratio in the hard block chains of the blended BCPs and the MAA copolymerization ratio in the methacrylate matrix polymer were varied. Without MAA copolymerization in the methacrylate matrix polymer, the 5 wt% BCP blends showed macroscopic phase separation, as shown in the TEM images in Figure 4. In contrast, nanostructures were observed when both the 5 wt% BCPs and the methacrylate polymer matrices had functional groups, as shown in Figure 5 and Figure 6. The relatively dark domains are PLMA nanophases stained with RuO$_4$. With decreasing amount of functional groups in both the matrix polymers and the hard block chains of the BCPs, the continuity of the PLMA nanophases increased from spherical micelles to worm-like cylindrical micelles, to long cylindrical micelles, shown in Figure 5 for 1.5 mol% copolymerized MAA and in Figure 6 for 3 mol% copolymerized MAA. The same trend in the continuity of the nano-micelles was observed in the 10 wt% BCP blends, as shown in Figure 7. The 10 wt% 'G22M78bL' BCP/3 mol% MAA copolymerized methacrylate polymer blends showed a curved lamellar nanostructure, with high continuity and reduced interfacial curvature.

A plausible mechanism for nanostructure formation during the polymerization process of the methacrylate monomer/BCP blends is as follows. When the methacrylate polymer matrices have no functional groups, the BCPs are macroscopically phase separated from the methacrylate polymer matrices during the polymerization process. In fact, polymerization-induced phase separation occurred in these cases. When the methacrylate polymer matrices have carboxy functional groups, the hard block chains with glycidyl groups of the BCPs are compatible with the MAA copolymerized methacrylate polymer matrices, and therefore the hard block chains can diffuse into the matrix. As the amount of glycidyl groups in the hard block chains increases, the compatibility of the hard block chains with the polymethacrylate matrices also increases. This leads to an increase in the curvature of the interfaces between the matrix and
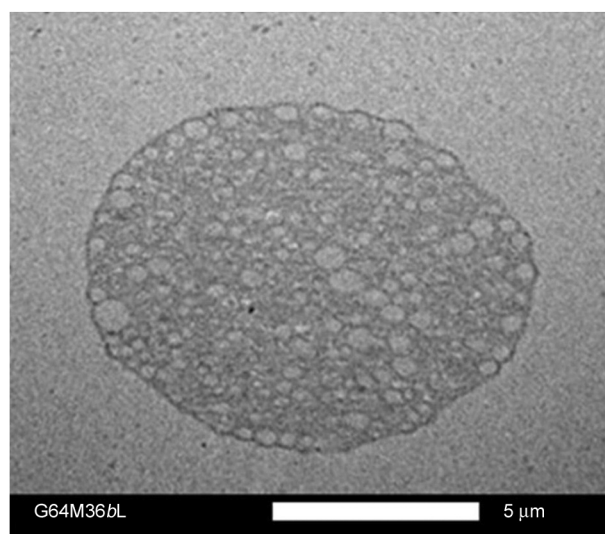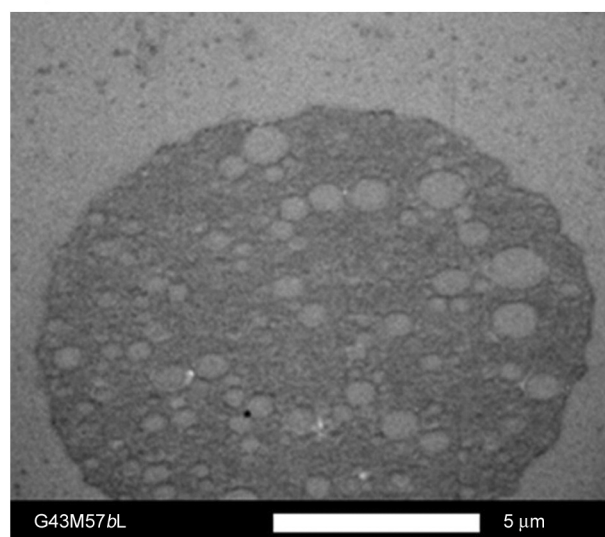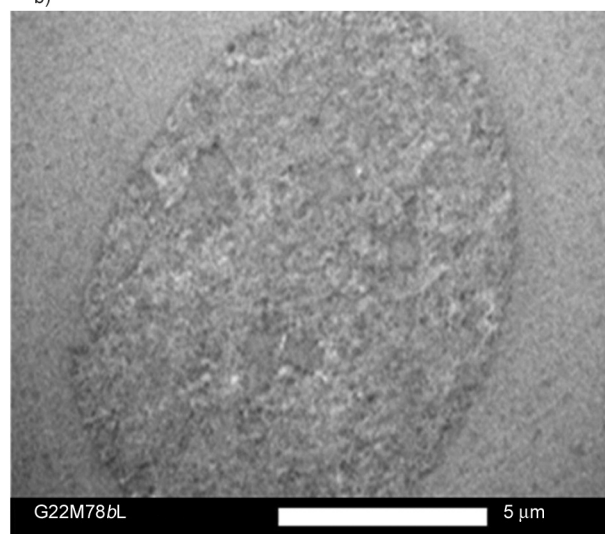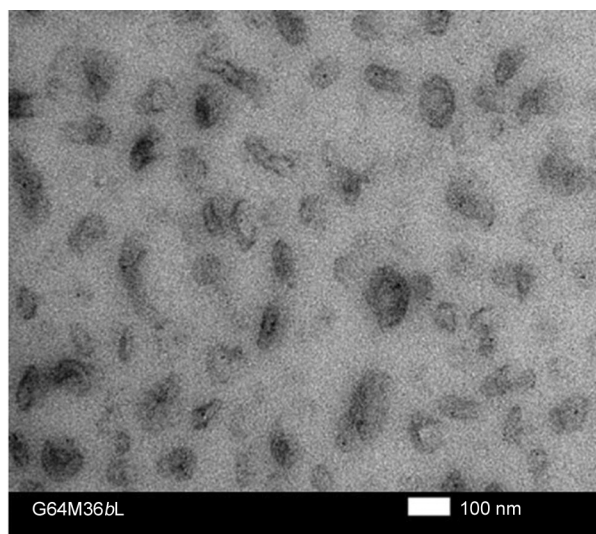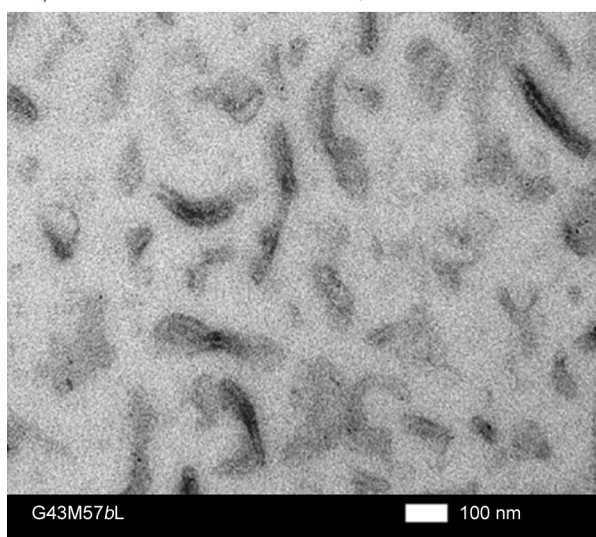
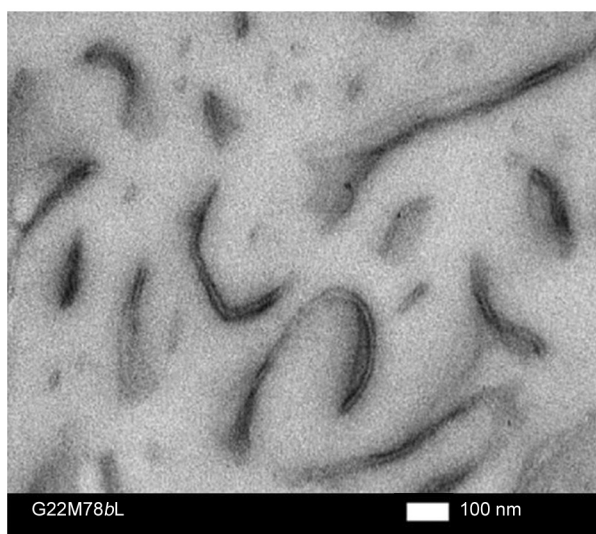**Figure 4.** TEM images of 5 wt% BCP/PMMA polymer blends (without MAA copolymerization) in the case of different BCPs: a) G64M36*b*L, b) G43M57*b*L, c) G22M78*b*L.
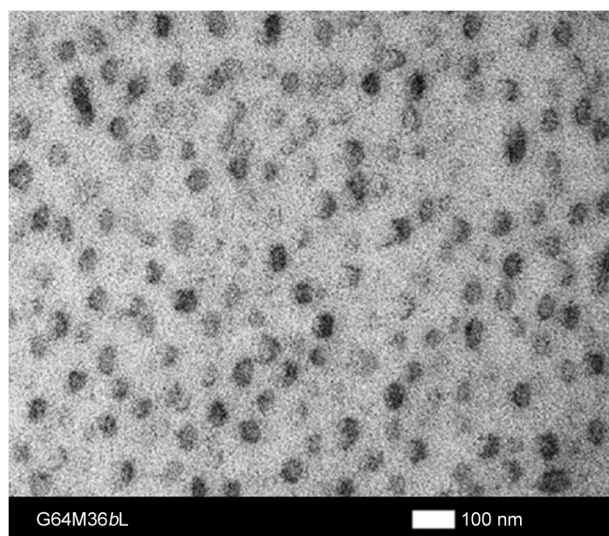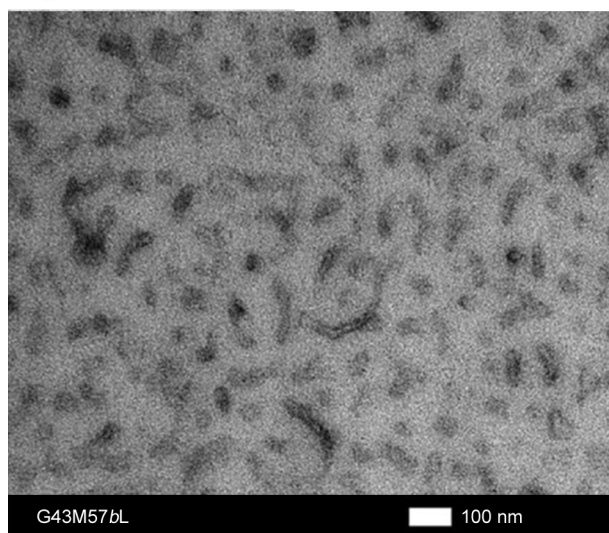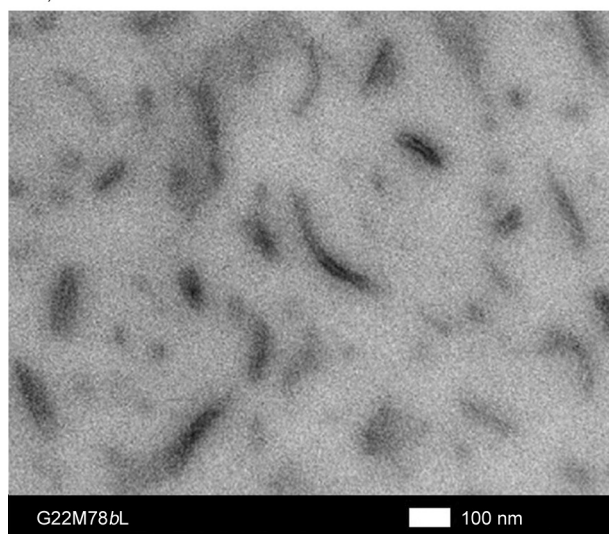
Figure 5. TEM images of 5 wt% BCP / methacrylate polymer blends with 1.5 mol% MAA copolymerization, in the case of different BCPs: a) G64M36*b*L, b) G43M57*b*L, c) G22M78*b*L.

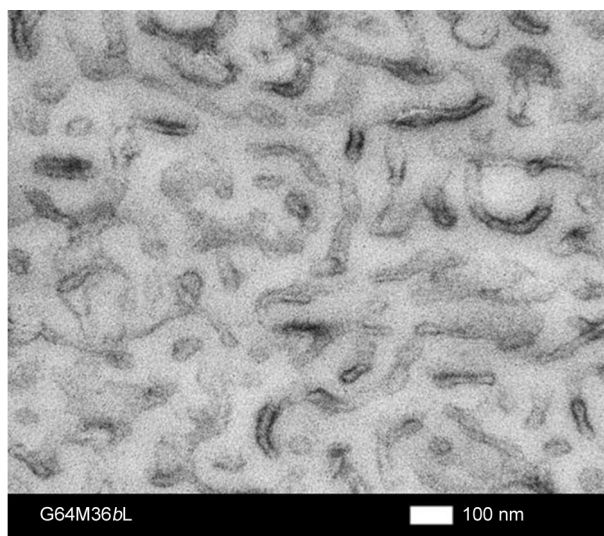**Figure 6.** TEM images of 5 wt% BCP / methacrylate polymer blends with 3 mol% MAA copolymerization, in the case of different BCPs: a) G64M36*b*L, b) G43M57*b*L, c) G22M78*b*L.
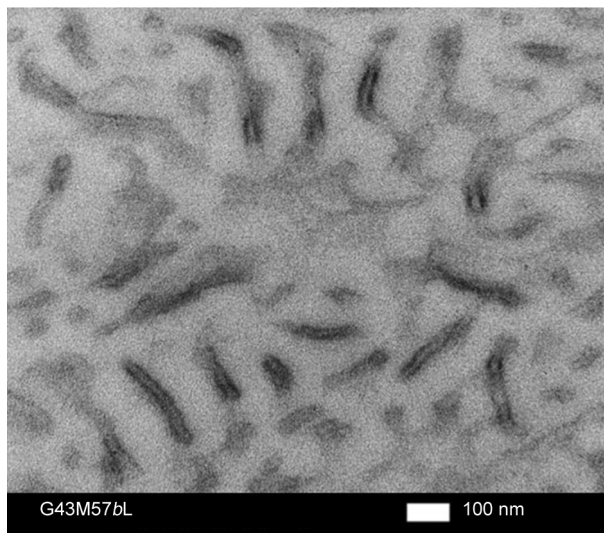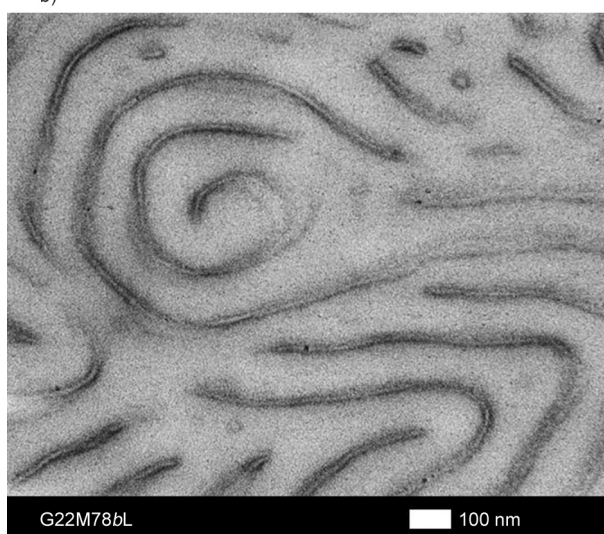
Figure 7. TEM images of 10 wt% BCP / methacrylate polymer blends with 3 mol% MAA copolymerization, in the case of different BCPs: a) G64M36*b*L, b) G43M57*b*L, c) G22M78*b*L.

the immiscible PLMA domains (soft block chains of the BCPs), thus forming spherical micelles. As the compatibility of the hard block chains with the matrix decreases, the hard block chains in the matrix shrink and the curvature of the interface between the matrix and the immiscible PLMA domains decreases. In fact, the difference in the compatibility of the hard block chains of the BCPs with the polymerized matrices is the key factor in determining the interfacial curvature and controlling the types of nano-micelles, such as spherical, worm-like cylindrical and curved lamellar. Several studies on epoxy polymer/ BCP blends [18, 26, 27] support the idea that 'the difference in compatibility between the BCP hard block chain and the matrix polymer affects the extent to which the hard block chain spreads into the matrix changes, which in turn changes the curvature of the micelle interface and the micelle morphology'. Yamada and Kishi [27] controlled the amount of carboxyl groups generated *in situ* on BCP hard block chains by varying the temperature and time of the mixing process and clarified the relationship between the amount of carboxyl groups and the micelle morphology generated in the epoxy blend.

3.3. Fracture toughness of MMA-MAA copolymerized matrix/functional BCP blends

The toughening effect of the MMA-MAA/functional BCP copolymerized blends with different nanostructures was evaluated. In Figure 8, the horizontal axis is the BCP content in the blends. First, the MAA copolymerization ratio in the matrix was kept at 3 mol%, and the GMA copolymerization ratio in the BCP hard block chains and the BCP content were

Figure 8. Fracture toughness, K_{IC}, for functional BCP/MMA-3 mol% MAA matrix copolymerized blends.

varied. The K_{IC} for the 5 wt% G22M78bL blends with worm-like cylindrical nano-micelles was very high, reaching 2.9 MPa·m$^{1/2}$. The K_{IC} for the 5 wt% G64M36bL blends with spherical nano-micelles was 1.4 MPa·m$^{1/2}$, which represented a marginal increase in toughness compared to pure PMMA (1.3 MPa·m$^{1/2}$). The K_{IC} for the 10 wt% G22M78bL blends with curved lamellar nano-micelles was 1.3 MPa·m$^{1/2}$, which meant almost no increase in toughness compared to pure PMMA.

The blends with worm-like cylindrical nano-micelles (5 wt% G22M78bL blend) showed characteristically high fracture toughness, even though the BCP content was lower than that for the curved lamellar structure (10 wt% G22M78bL blend). In fact, the fracture toughness, KIC, for the blends depended on the type of nanostructure rather than on the amount of BCPs blended.

Figure 9 shows the fracture surfaces of the 5 wt% G64M36bL/MMA-3 mol% MAA copolymerized blend with spherical nano-micelles and the 5 wt% G22M78bL/MMA-3 mol% MAA copolymerized blend with worm-like cylindrical nano-micelles after the fracture toughness evaluation. Although both blends contained the same amount of PLMA soft block chains with the same molecular weight, the fracture surface roughness of the blend with worm-like cylindrical nano-micelles (Figure 9b) was much higher than that of the blend with spherical nano-micelles (Figure 9a). The PLMA micelles in the present study are elastomeric phases. The difference in roughness is due to the different extent of cavitation of the elastomeric phases and plastic deformation of the polymethacrylate matrix during the fracture process. In fact, the nanocavities on the fracture surfaces observed in Figure 9b originated from the worm-like cylindrical nano-micelles of PLMA in the blends. As such, the observed plastic deformation around the nanocavities results from yielding and elongation of the polymethacrylate matrix. As is well known, however, the information obtained from fracture surface observations is limited, considering the internal deformation and overall fracture events of the specimens [36–39]. Therefore, side-view observations were carried out to investigate and compare the extent of different types of deformations that would be generated in the deformation process zone in front of a pre-crack tip in the nanostructured blends, as described in the next section.
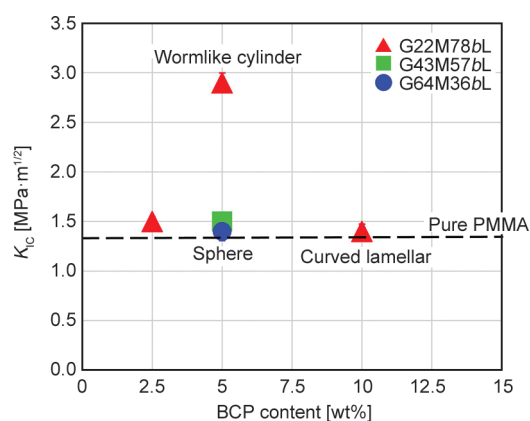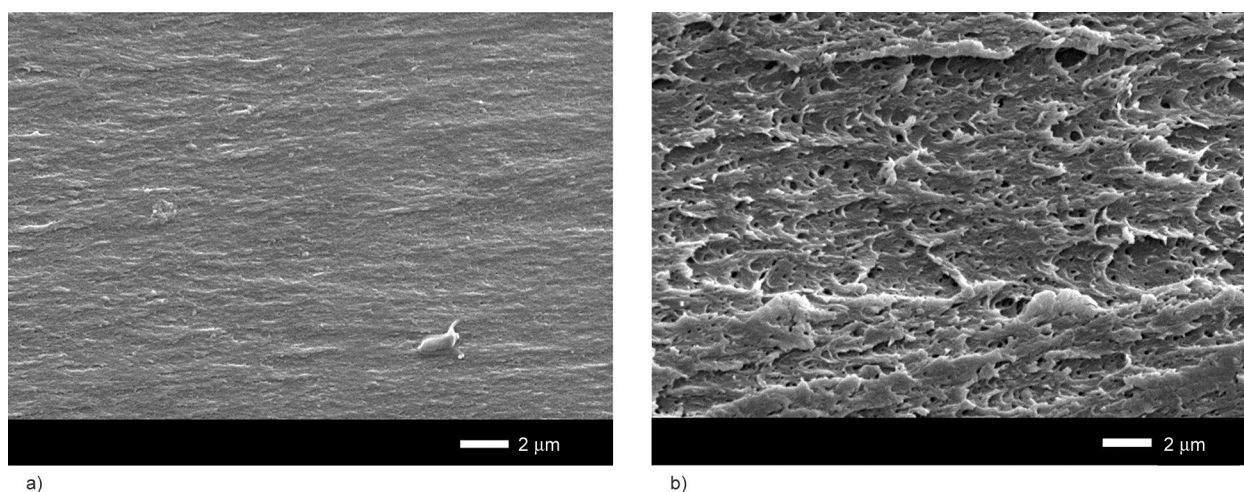
Figure 9. Fracture surfaces after K_{IC} evaluation of 5 wt% functional BCP/MMA-3 mol% MAA copolymerized blends observed using SEM. a) 5 wt% G64M36*b*L/MMA-3 mol% MAA copolymerized blend with spherical nano-micelles; b) 5 wt% G22M78*b*L/MMA-3 mol% MAA copolymerized blend with worm-like cylindrical nano-micelles.

3.4. Toughening mechanisms of MMA-MAA/functional BCP copolymerized blends

Double-notched four-point bending (DN-4PB) tests were carried out to elucidate the toughening mechanisms. Polished thin sections were taken from the mid-plane of the test specimens, including the deformation region in front of the subcritical crack tip [36, 37]. The deformation process zones were then observed as side-views, perpendicular to the fracture surface, by OM in both bright-field and cross-polarized modes. Figure 10 shows the blends with worm-like cylindrical nano-micelles with a K_{IC} value of 2.9 MPa·m$^{1/2}$. Figure 11 shows the blends with spherical nano-micelles with a K_{IC} value of 1.4 MPa·m$^{1/2}$. A large difference in the size of the deformation zones can be seen. The blends with worm-like cylindrical nano-micelles showed a much larger process zone than the blends with spherical nano-micelles. Elliptical regions of high birefringence were observed in the deformation process zone of the blends with worm-like cylindrical nano-micelles in cross-polarized mode in Figure 10. This means that very large plastic deformation, shear yielding, took place in the blends with worm-like cylindrical micelles. The maximum thickness of the shear yield zone reached more than 300 µm. Deformation regions, which look like fine hairs, can also be seen around the elliptical plastic deformation region. On the other hand, for the blends with spherical nano-micelles, no region of birefringence is clearly visible in Figure 11.
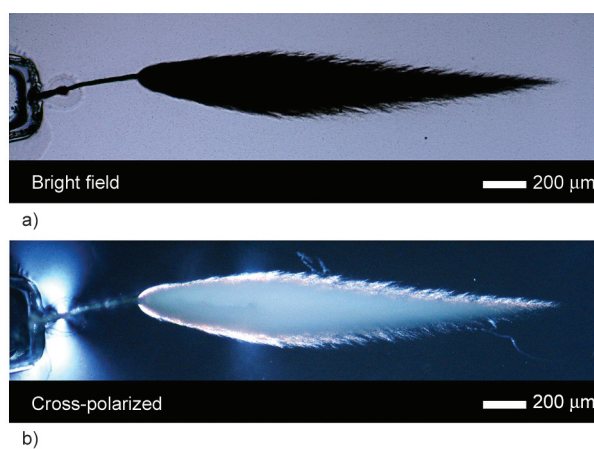

Figure 10. OM images of deformation process zones of 5 wt% G22M78*b*L/MMA-3 mol% MAA copolymerized blend with worm-like cylindrical nano-micelles in transmission bright-field (a) and cross-polarized (b) modes.
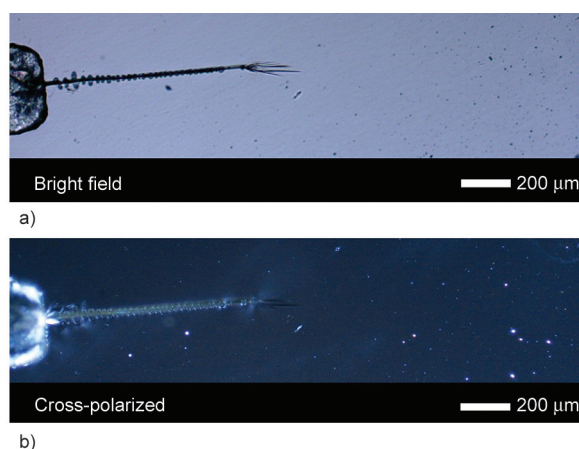

Figure 11. OM images of deformation process zones of 5 wt% G64M36*b*L/MMA-3 mol% MAA copolymerized blend with spherical nano-micelles in transmission bright-field (a) and cross-polarized (b) modes.
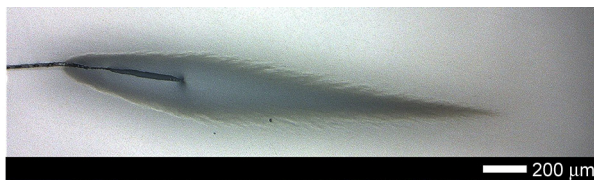
Figure 12. OM photograph of the deformation process zone of the 5 wt% G22M78bL/MMA-3 mol% MAA copolymerized blend with worm-like cylindrical nano-micelles observed under reflected light mode.

Figure 12 shows the same sample of the blend with the worm-like cylindrical nano-micelles observed in reflection mode using OM. Crack propagation of approximately 400 μm in length can be seen in the elliptical deformation zone. In addition, a slightly shaded area appeared around the fine hair-like deformation region outside the shear yielding region. The above observation raises the question as to what happened outside the elliptical deformation region, in the fine hair-like deformation region, and in the shear yielding region within the elliptical deformation region.

More detailed TEM observations were carried out on the same areas of the two blends with the worm-like cylindrical nano-micelles (Figures 13–17) and the spherical nano-micelles (Figure 18 and Figure 19). Figure 13 shows a TEM image of the area outside the elliptical deformation zone, which is approximately 900 μm from the propagating crack tip. Cavitated and non-cavitated worm-like cylinders are seen to co-exist outside the elliptical deformation zone far from the crack tip.

Figure 14 shows the hair-like deformation region approximately 300 μm from the propagating crack tip, which is closer to the crack tip than the region in Figure 13. Some continuity and change in orientation of the cavitated worm-like cylinders towards the load direction due to the increased stress can be observed.

Figure 15 shows the hair-like deformation region approximately 150 μm from the propagating crack tip. The continuity of the cavitated worm-like nano-cylinder has increased and the size of the cavities has also increased. This is described as a 'craze-like' deformation region [40–42].

Figure 16 shows the shear yielding region within the elliptical deformation zone, approximately 70 μm from the propagating crack tip. The size of the continuous cavitation of the worm-like cylindrical micelles is increased and elongated ligaments (polymethacrylate matrix) are observed between the cavities, corresponding to shear yielding. The aligned cavitation region exhibits 'craze-like' deformation with increasing load.
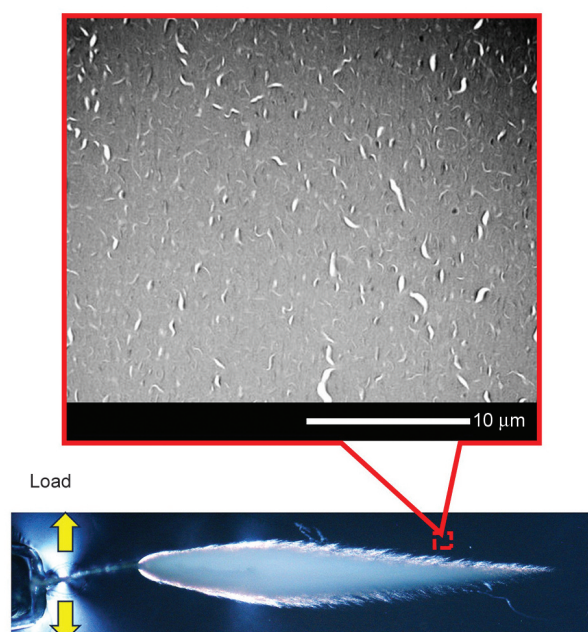

Figure 13. TEM image of deformation process zone of 5 wt% G22M78bL/MMA-3 mol% MAA copolymerized blend with worm-like cylindrical nano-micelles. The area is outside the elliptical deformation region, which is approximately 900 μm from the propagating crack tip.

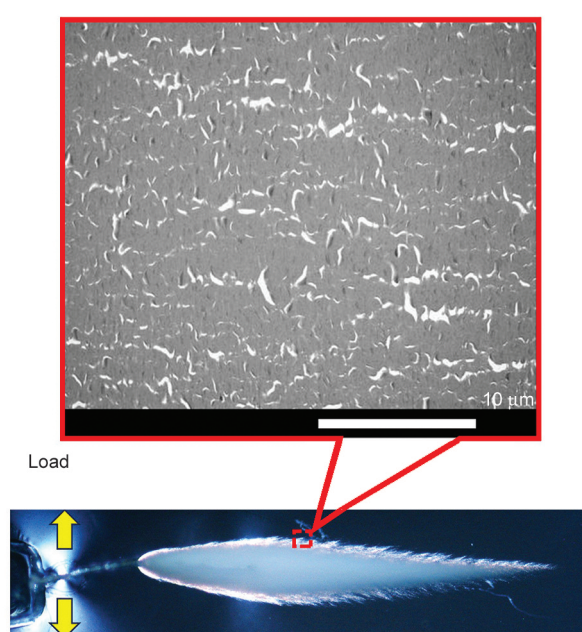**Figure 14.** TEM image of deformation process zone of 5 wt% G22M78bL/MMA-3 mol% MAA copolymerized blend with worm-like cylindrical nano-micelles. The image shows the hair-like deformation region, approximately 300 μm from the propagating crack tip.

Figure 15. TEM image of deformation process zone of 5 wt% G22M78*b*L/MMA-3 mol% MAA copolymerized blend with worm-like cylindrical nano-micelles. The image shows the hair-like deformation region, approximately 150 μm from the propagating crack tip.

Figure 16. TEM image of deformation process zone of 5 wt% G22M78*b*L/MMA-3 mol% MAA copolymerized blend with worm-like cylindrical nano-micelles. The image shows the hair-like deformation region, approximately 70 μm from the propagating crack tip.
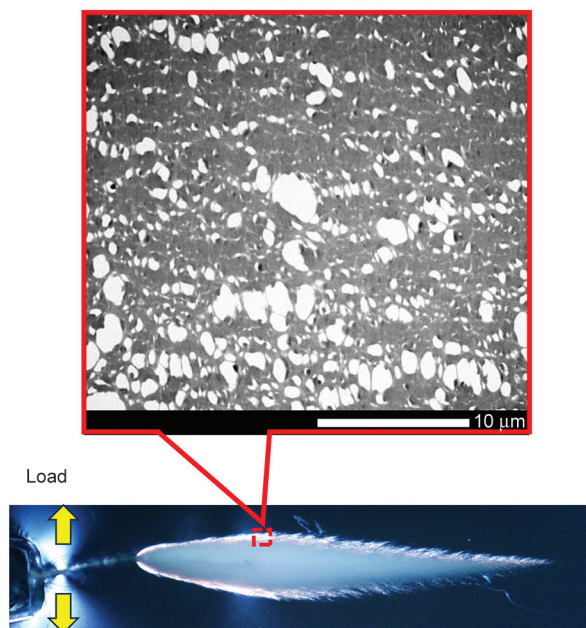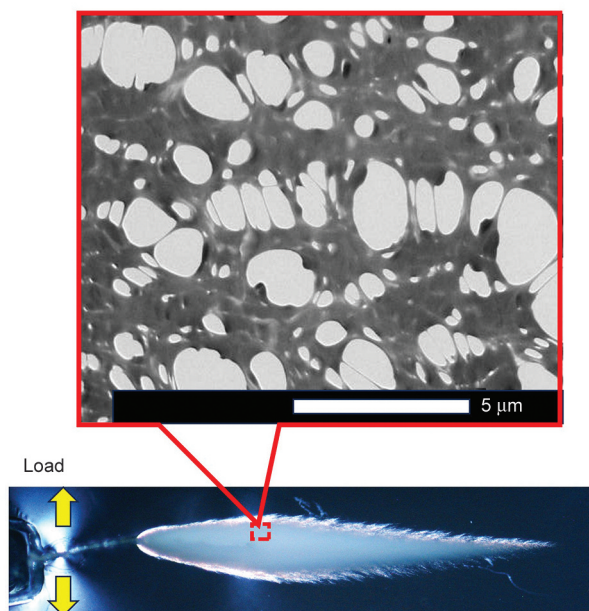
In summary, cavitation of worm-like cylindrical nano-micelles composed of PLMA, followed by craze-like deformation, and large shear yielding of the polymethacrylate matrix were identified as the
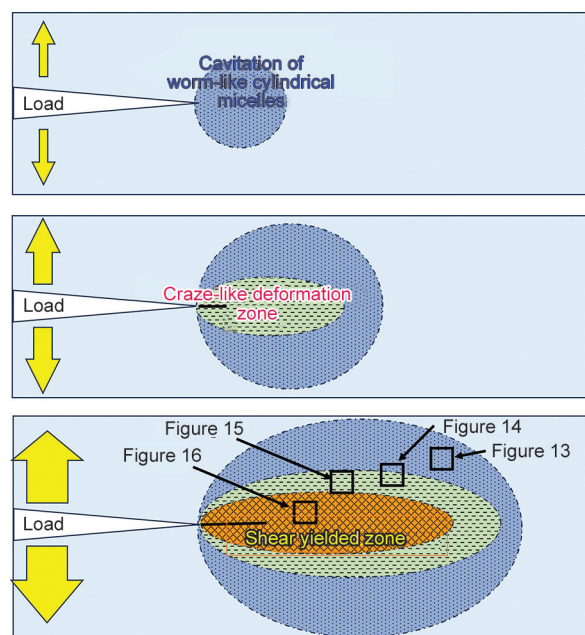

Figure 17. Schematic illustration of sequence of deformation events under loading in 5 wt% G22M78*b*L/ MMA-3 mol% MAA copolymerized blend with worm-like cylindrical nano-micelles.

deformation processes that contribute to toughening of blends with worm-like cylindrical nano-micelles. The stress induced by the load decreased with increasing distance from the crack tip. Therefore, phenomena observed at locations relatively far from the crack tip should occur when the load is small, and the phenomena occurring as the load increases should be observed closer to the crack tip. From this point of view, the following toughening mechanisms are considered: (1) Nanocavitation of the PLMA elastomeric worm-like cylindrical phase first occurs in front of the crack tip. (2) Subsequently, the cavitated worm-like nanocylinders form craze-like deformation bands including massive cavitation. (3) The massive cavitation in the craze-like deformation zone can relieve the hydrostatic tensile (dilatational) stress in front of the crack tip [43–45]. As a result, a large shear yielded zone is formed in the craze-like deformation zone. The large shear yield, which absorbs a lot of strain energy, delays main crack propagation, and contributes to the very high fracture toughness [46, 47]. This sequence of deformation events is illustrated schematically in Figure 17.

Multiple failure mechanisms, including the coexistence of or competition between craze and shear yielding, have been reported for toughened bio-based polyamide 410 blends by Samantaray *et al.* [48]. However, they used notched thin specimens under

plane stress conditions. In this study, we used notched thick specimens under plane strain conditions. Therefore, the difference in stress state would result in a different sequence of deformation events contributing to the toughening mechanisms.

For blends with spherical nano-micelles, the birefringence indicating shear yielding was very limited, and some deformation lines can be seen in front of the crack tip using OM as shown in Figure 11. More detailed TEM observations were carried out on the same areas of the blend with the spherical nano-micelles. Figure 18 shows an area approximately 80 μm from the crack tip. Very localized 'craze-like' deformation bands are observed. The size of the cavitation of the nanospheres in the blend was small compared to the blends with the worm-like cylindrical nano-micelles.
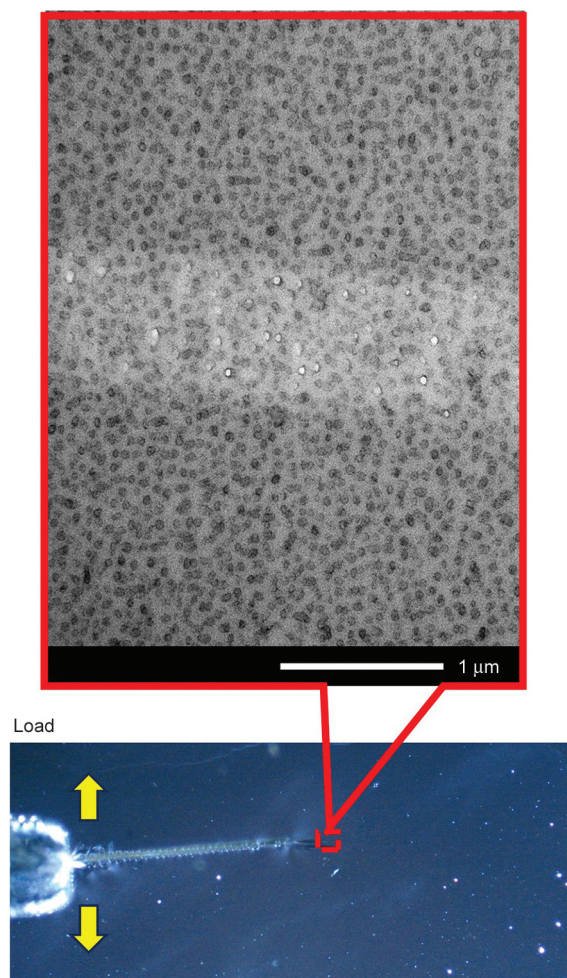
In Figure 19, a small number of elongated micelles can be observed in the craze-like deformation bands near the crack tip, although the initial nano-micelles were spherical. This means that the methacrylate polymer matrix was plastically deformed in a very confined region adjacent to the craze-like deformation bands near the crack tip. In summary, the cavitation and craze-like deformation bands were very localized and confined in the case of the blends containing spherical nano-micelles. As a result, shear yielding was also limited very close to the crack tip. Therefore, the very limited plastic deformation was not clearly visible in Figure 11 under OM, and the toughening effect was marginal.

The next research question is to explain the difference in cavitation resistance between the two different types of nano-micelles. The cavitation resistance

Figure 18. TEM images of deformation process zone of 5 wt% G64M36*b*L/MMA-3 mol% MAA copolymerized blend with spherical nano-micelles. The area is approximately 80 μm from the crack tip. Craze-like deformation bands propagated from left to right.
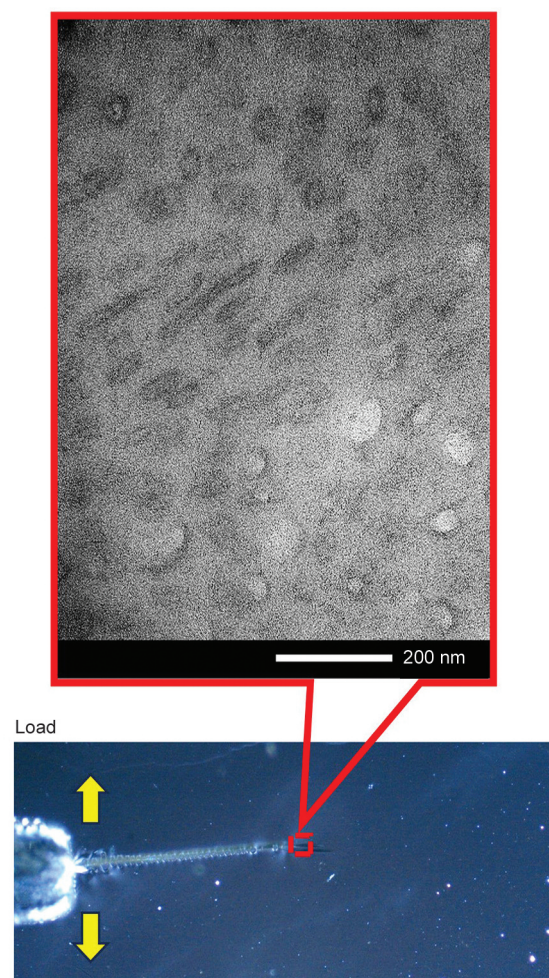
Figure 19. TEM images of deformation process zone of 5 wt% G64M36bL/MMA-3 mol% MAA copolymerized blend with spherical nano-micelles, in craze-like deformation bands very close to the crack tip.

of the spherical nano-micelles is higher than that of the worm-like cylindrical micelles, although both types of micelles are composed of PLMA with the same molecular weight. One of the factors influencing the cavitation resistance could be the difference in the size of the micelles. Previous studies of rubber-reinforced resins have shown that the larger the particles, the lower the cavitation resistance, even when the rubber particles are of the same material [32, 49]. In the present study, the worm-like cylindrical micelles were larger than the spherical nano-micelles. A detailed study of the factors that dominate the cavitation resistance will be performed in the future.

4. Conclusions

Lightly cross-linked nanostructured methacrylate polymer/BCP blends were obtained by redox-type radical polymerization of MMA and MAA in the presence of BCPs and *in situ* reaction of the carboxy groups of the matrix monomers with the glycidyl groups in the BCP hard blocks. The curvature of the interface between the nano-micelles and the polymethacrylate matrices was found to be a key factor in controlling the types of nanostructures, such as spherical, worm-like cylindrical and curved lamellar, of the methacrylate polymer/BCP blends.

The fracture toughness of the blends depended on the nanostructures. The blends with worm-like cylindrical nano-micelles showed the highest toughness. Craze-like deformation occurred due to cavitation initiated at the worm-like cylindrical PLMA nano-micelles in the matrix of the polymethacrylate/BCP blends. The massive cavitation in the craze-like deformation zone relieved the hydrostatic tensile stress in front of the crack tip. As a result, a large shear yielded zone was formed within the region of the craze-like deformation, which contributed to the very high fracture toughness.

Acknowledgements

References
[1] Ali U., Karim K., Buang N.: A review of the properties and applications of poly (methyl methacrylate) (PMMA). Polymer Reviews, **55**, 678–705 (2015).
https://doi.org/10.1080/15583724.2015.1031377

[2] Zheng B., Zhang S., Shu G., Sun Z., Wang Y., Xie J.: Experimental investigation and modeling of the mechanical properties of construction PMMA at different temperatures. Structures, **57**, 105091 (2023).
https://doi.org/10.1016/j.istruc.2023.105091

[3] Zafar M. S.: Prosthodontic applications of polymethyl methacrylate (PMMA): An update. Polymers, **12**, 2299 (2020).
https://doi.org/10.3390/polym12102299

[4] Lovell P. A., McDonald J., Saunders D. E. J., Young R. J.: Studies of rubber-toughened poly(methyl methacrylate): 1. Preparation and thermal properties of blends of poly(methyl methacrylate) with multiple-layer toughening particles. Polymer, **34**, 61–69 (1993).
https://doi.org/10.1016/0032-3861(93)90284-h

[5] Gloaguen J. M., Steer P., Gaillard P., Wrotecki C., Lefebvre J. M.: Plasticity and fracture initiation in rubber-toughened poly(methyl methacrylate). Polymer Engineering and Science, **33**, 748–753 (1993).
https://doi.org/10.1002/pen.760331205

[6] Plummer C. J. G., Béguelin P., Kausch H-H.: On the influence of particle morphology on microdeformation in rubber modified poly(methyl methacrylate). Polymer, **37**, 7–10 (1996).
https://doi.org/10.1016/0032-3861(96)81593-X

[7] Cho K., Yang J., Park C. E.: The effect of interfacial adhesion on toughening behaviour of rubber modified poly(methyl methacrylate). Polymer, **38**, 5161–5167 (1997).
https://doi.org/10.1016/S0032-3861(97)00052-9

[8] Cho K., Yang J., Park C. E.: The effect of rubber particle size on toughening behaviour of rubber-modified poly(methyl methacrylate) with different test methods. Polymer, **39**, 3073–3081 (1998).
https://doi.org/10.1016/S0032-3861(97)10036-2

[9] Suto H., Yoda K., Watanabe J., Yang L.: Development of the low-odor and non-flammable second-generation acrylic adhesive and its applications. Journal of Adhesion Society of Japan, **48**, 127–136 (2012).
https://doi.org/10.11618/adhesion.48.127

[10] Hayashi A., Sekiguchi Y., Sato C.: AFM observation of sea-island structure formed by second generation acrylic adhesive. Journal of Adhesion, **97**, 155–171 (2021).
https://doi.org/10.1080/00218464.2019.1649148

[11] Kamiyama K., Mikuni M., Matsumoto T., Matsuda S., Kishi H.: Crack growth mechanism on SGA adhesive joints. International Journal of Adhesion and Adhesives, **103**, 102690 (2020).
https://doi.org/10.1016/j.ijadhadh.2020.102690

[12] Bucknall C. B., Smith R. R.: Stress-whitening in high-impact polystyrenes. Polymer, **6**, 437–446 (1965).
https://doi.org/10.1016/0032-3861(65)90028-5

[13] Matsuo M.: Fine structures and fracture processes in plastic/rubber two-phase polymer systems. II. Observation of crazing behaviors under the electron microscope. Polymer Engineering and Science, **9**, 206–212 (1969).
https://doi.org/10.1002/pen.760090309

[14] Kambour R. P.: A review of crazing and fracture in thermoplastics. Journal of Polymer Science, Macromolecular Reviews, **7**, 1–154 (1973).
https://doi.org/10.1002/pol.1973.230070101

[15] Socrate S., Boyce M. C., Lazzeri A.: A micromechanical model for multiple crazing in high impact polystyrene. Mechanics of Materials, **33**, 155–175 (2001).
https://doi.org/10.1016/S0167-6636(00)00068-5

[16] Sharma R., Socrate S.: Micromechanics of uniaxial tensile deformation and failure in high impact polystyrene (HIPS). Polymer, **50**, 3386–3395 (2009).
https://doi.org/10.1016/j.polymer.2009.04.073

[17] Hillmyer M. A., Lipic P. M., Hajduk D. A., Almdal K., Bates F. S.: Self-assembly and polymerization of epoxy resin-amphiphilic block copolymer nanocomposites. Journal of the American Chemical Society, **119**, 2749–2750 (1997).
https://doi.org/10.1021/ja963622m

[18] Lipic P. M., Bates F. S., Hillymer M. A.: Nanostructured thermosets from self-assembled amphiphilic block copolymer/epoxy resin mixtures. Journal of the American Chemical Society, **120**, 8963–8970 (1998).
https://doi.org/10.1021/ja981544s

[19] Dean J. M., Grubbs R. B., Saad W., Cook R. F., Bates F. S.: Mechanical properties of block copolymer vesicle and micelle modified epoxies. Journal of Polymer Science. Part B: Polymer Physics, **41**, 2444–2456 (2003).
https://doi.org/10.1002/polb.10595

[20] Ritzenthaler S., Court F., David L., Girard-Reydet E., Leibler L., Pascault J. P.: ABC triblock copolymers/epoxy-diamine blends. 1. Keys to achieve nanostructured thermosets. Macromolecules, **35**, 6245–6254 (2002).
https://doi.org/10.1021/ma0121868

[21] Ritzenthaler S., Court F., Girard-Reydet E., Leibler L., Pascault J. P.: ABC triblock copolymers/epoxy-diamine blends. 2. Parameters controlling the morphologies and properties. Macromolecules, **36**, 118–126 (2003).
https://doi.org/10.1021/ma0211075

[22] Kishi H., Kunimitsu Y., Imade J., Oshita S., Morishita Y., Asada M.: Nano-phase structures and mechanical properties of epoxy/acryl triblock copolymer alloys. Polymer, **52**, 760–768 (2011).
https://doi.org/10.1016/j.polymer.2010.12.025

[23] Kishi H., Kunimitsu Y., Nakashima Y., Abe T., Imade J., Oshita S., Morishita Y., Asada M.: Control of nanostructures generated in epoxy matrices blended with PMMA-*b*-PnBA-*b*-PMMA triblock copolymers. Express Polymer Letters, **9**, 23–35 (2015).
https://doi.org/10.3144/expresspolymlett.2015.4

[24] Asada M., Oshita S., Morishita Y., Nakashima Y., Kunimitsu Y., Kishi H.: Effect of miscible PMMA chain length on disordered morphologies in epoxy/PMMA-*b*-PnBA-*b*-PMMA blends by *in situ* simultaneous SAXS/DSC. Polymer, **105**, 172–179 (2016).
https://doi.org/10.1016/j.polymer.2016.10.025

[25] Kishi H., Kunimitsu Y., Nakashima Y., Imade J., Oshita S., Morishita Y., Asada M.: Relationship between the mechanical properties of epoxy/PMMA-*b*-PnBA-*b*-PMMA block copolymer blends and their three-dimensional nanostructures. Express Polymer Letters, **11**, 765–777 (2017).
https://doi.org/10.3144/expresspolymlett.2017.74

[26] Kishi H., Yamada K., Kimura J.: Control of nanostructures and fracture toughness of epoxy/acrylic block copolymer blends using *in situ* manipulation of the epoxy matrix reaction type. Polymer, **176**, 89–100 (2019).
https://doi.org/10.1016/j.polymer.2019.05.024

[27] Yamada K., Kishi H.: Control of nanostructures in epoxy/acrylic block copolymer blends by the *in situ* generation of functional groups. Polymer Journal, **49**, 617–623 (2017).
https://doi.org/10.1038/pj.2017.26

[28] Liu J., Sue H-J., Thompson Z. J., Bates F. S., Dettloff M., Jacob G., Verghese N., Pham H.: Nanocavitation in self-assembled amphiphilic block copolymer-modified epoxy. Macromolecules, **41**, 7616–7624 (2008).
https://doi.org/10.1021/ma801037q

[29] Thompson Z. J., Hillymer M. A., Liu J., Sue H-J., Dettloff M., Bates F. S.: Block copolymer toughened epoxy: Role of cross-link density. Macromolecules, **42**, 2333–2335 (2009).
https://doi.org/10.1021/ma900061b

[30] Liu J., Thompson Z. J., Sue H-J., Bates F. S., Hillymer M. A., Dettloff M., Jacob G., Verghese N., Pham H.: Toughening of epoxies with block copolymer micelles of wormlike morphology. Macromolecules, **43**, 7238–7243 (2010).
https://doi.org/10.1021/ma902471g

[31] Ferry J. D.: Viscoelastic properties of polymers. Wiley, New York (1980).

[32] Nielsen L. I.: Mechanical properties of polymers and composites. Marcel Dekker, New York (1975).

[33] Murayama T., Bell J. P.: Relation between the network structure and dynamic mechanical properties of a typical amine-cured epoxy polymer. Journal of Polymer Science A2, **8**, 437–445 (1970).
https://doi.org/10.1002/pol.1970.160080309

[34] Urbaczewski-Espuche E., Gerard J. F., Pascault J. P., Reffo G., Sautereau H.: Toughness improvement of an epoxy/anhydride matrix. Influence on processing and fatigue properties of unidirectional glass–fiber composites. Journal of Applied Polymer Science, **47**, 991–1002 (1993).
https://doi.org/10.1002/app.1993.070470605

[35] Poonpipat Y., Leelachai K., Pearson R. A.: Dittanet P.: Fracture behavior of silica nanoparticles reinforced rubber/epoxy composite. Journal of Reinforced Plastics and Composites, **36**, 1156–1167 (2017).
https://doi.org/10.1177/0731684417709952

[36] Sue H-J., Huang J., Yee A. F.: Interfacial adhesion and toughening mechanisms in an alloy of polycarbonate/polyethylene. Polymer, **33**, 4868–4871 (1992).
https://doi.org/10.1016/0032-3861(92)90707-4

[37] Sue H-J., Yee A. F.: Study of fracture mechanisms of multiphase polymers using the double-notch four-point-bending method. Journal of Materials Science, **28**, 2975–2980 (1993).
https://doi.org/10.1007/BF00354702

[38] Pearson R. E., Yee A. F.: Toughening mechanisms in elastomer-modified epoxies, Part 2: Microscopy studies. Journal of Materials Science, **21**, 2475–2488 (1986).
https://doi.org/10.1007/BF01114294

[39] Pearson R. E., Yee A. F.: Toughening mechanisms in elastomer-modified epoxies, Part 3: The effect of crosslink density. Journal of Materials Science, **24**, 2571–2580 (1989).
https://doi.org/10.1007/BF01174528

[40] Sue H-J.: Craze-like damage in a core-shell rubber-modified epoxy system. Journal of Materials Science, **27**, 3098–3107 (1992).
https://doi.org/10.1007/BF01154125

[41] Sue H-J., Garcia-Mertin E. I., Orchard N. A.: Toughening of epoxies via craze-like damage. Journal of Polymer Science. Part B: Polymer Physics, **31**, 595–608 (1993).
https://doi.org/10.1002/polb.1993.090310511

[42] Sue H-J., Bertram J. L., Garcia-Mertin E. I., Wilchester J. W., Walker L. L.: Fracture behavior of core-shell rubber-modified crosslinkable epoxy thermoplastics. Colloid and Polymer Science, **272**, 456–466 (1994).
https://doi.org/10.1007/BF00659459

[43] Sue H-J., Yee A. F.: Toughening mechanisms in a multi-phase alloy of nylon 6,6/polyphenylene oxide. Journal of Materials Science, **24**, 1447–1457 (1989).
https://doi.org/10.1007/BF02397085

[44] Yee A. F., Li D., Li X.: The importance of constraint relief caused by rubber cavitation in the toughening of epoxy. Journal of Materials Science, **28**, 6392–6398 (1993).
https://doi.org/10.1007/BF01352202

[45] Kishi H., Shi Y-B., Huang J., Yee A. F.: Ductility and toughenability study of epoxy resins under multiaxial stress states. Journal of Materials Science, **33**, 3479–3488 (1998).
https://doi.org/10.1023/A:1013222421843

[46] Narisawa I., Yee A. F.: Crazing and fracture of polymers. in 'Materials science and technology' Wiley, Weinheim, 701–765 (2006).
https://doi.org/10.1002/9783527603978.mst0146

[47] Yee A. F., Harcup J., Narisawa I.: Strength, fracture and fatigue of polymers. Academic Press, New York (2012).

[48] Samantaray S. K., Thakur V., Satapathy B. K.: On strain-rate independent fracture toughness and relaxation in cyclic tensile behavior: A case study for toughened biobased polyamide 410 blends. Materialia, **24**, 101490 (2022).
https://doi.org/10.1016/j.mtla.2022.101490

[49] Lazzeri A., Bucknall C. B.: Dilatational bands in rubber-toughened polymers. Journal of Materials Science, **28**, 6799–6808 (1993).
https://doi.org/10.1007/BF00356433